Thermal Design and Analysis of the Supersonic Flight Dynamics Test Vehicle for the Low Density Supersonic Decelerator Project

A. J. Mastropietro[1], Dr. Michael Pauken[2], Eric Sunada[3], and Sandria Gray[4]
Jet Propulsion Laboratory, California Institute of Technology, Pasadena, California, 91109

The thermal design and analysis of the experimental Supersonic Flight Dynamics Test (SFDT) vehicle is presented. The SFDT vehicle is currently being designed as a platform to help demonstrate key technologies for NASA's Low Density Supersonic Decelerator (LDSD) project. The LDSD project is charged by NASA's Office of the Chief Technologist (OCT) with the task of advancing the state of the art in Mars Entry, Descent, and Landing (EDL) systems by developing and testing three new technologies required for landing heavier payloads on Mars. The enabling technologies under development consist of a large 33.5 meter diameter Supersonic Ringsail (SSRS) parachute and two different types of Supersonic Inflatable Aerodynamic Decelerator (SIAD) devices – a robotic class, SIAD-R, that inflates to a 6 meter diameter torus, and an exploration class, SIAD-E, that inflates to an 8 meter diameter isotensoid. As part of the technology development effort, the various elements of the new supersonic decelerator system must be tested in a Mars-like environment. This is currently planned to be accomplished by sending a series of SFDT vehicles into Earth's stratosphere. Each SFDT vehicle will be lifted to a stable float altitude by a large helium carrier balloon. Once at altitude, the SFDT vehicles will be released from their carrier balloon and spun up via spin motors to provide trajectory stability. An onboard third stage solid rocket motor will propel each test vehicle to supersonic flight in the upper atmosphere. After main engine burnout, each vehicle will be despun and testing of the deceleration system will begin: first an inflatable decelerator will be deployed around the aeroshell to increase the drag surface area, and then the large parachute will be deployed to continue the deceleration and return the vehicle back to the Earth's surface. The SFDT vehicle thermal system must passively protect the vehicle structure and its components from cold temperatures experienced during the ascent phase of the mission as well as from the extreme heat fluxes produced during the supersonic test phase by the main motor plume and aeroheating. The passive thermal design approach for the SFDT vehicle relies upon careful and complex bounding analysis of all three modes of heat transfer - conduction, convection, and radiation - coupled with a tightly managed transient power dissipation timeline for onboard electronics components throughout all mission phases.

Nomenclature

AFT	=	Allowable Flight Temperature
ARC	=	NASA Ames Research Center
BLDT	=	Balloon Launched Decelerator Test
CBE	=	Current Best Estimate
CFD	=	Computational Fluid Dynamics
CSA	=	Core Structure Assembly
CSBF	=	NASA Columbia Scientific Balloon Facility
EDL	=	Entry, Descent, and Landing

[1] Thermal Systems Engineer, Thermal and Fluids System Engineering Group.
[2] Senior Thermal Systems Engineer, Thermal and Fluids System Engineering Group.
[3] Group Supervisor, Propulsion, Thermal, and Materials Engineering Section.
[4] Thermal Systems Engineer, Instrument Thermal Engineering Group.

IR	=	Infrared
JPL	=	NASA Jet Propulsion Laboratory
LDSD	=	Low Density Supersonic Decelerator
MLI	=	Multi-Layer Insulation
MSFC	=	NASA Marshall Spaceflight Center
MSL	=	Mars Science Laboratory
NASA	=	National Aeronautics and Space Administration
OCT	=	NASA Office of the Chief Technologist
PBE	=	Probable Best Estimate
PDD	=	Parachute Deployment Device
PMRF	=	U. S. Navy Pacific Missile Range Facility
SFA	=	Shoulder Fairing Assembly
SFDT	=	Supersonic Flight Dynamics Test
SIAD-E	=	Supersonic Inflatable Aerodynamic Decelerator, Exploration Class
SIAD-R	=	Supersonic Inflatable Aerodynamic Decelerator, Robotic Class
SSRS	=	Supersonic Ringsail (Parachute)
TPS	=	Thermal Protection System
WCH	=	Worst Case Hot
WCC	=	Worst Case Cold
WFF	=	NASA Wallops Flight Facility

I. Introduction

NASA has used technology developed for the Viking Program in the early 1970s for every mission landing payloads on Mars including most recently, the Mars Science Laboratory (MSL) in 2012. In order to land payloads at higher elevations or with heavier mass than currently possible, new parachute and aerodynamic decelerator technologies must be developed. This paper describes the thermal design and analysis of the Supersonic Flight Dynamics Test (SFDT) vehicles that are currently being developed for NASA's Low Density Supersonic Decelerator (LDSD) project. The LDSD project is charged by NASA's Office of the Chief Technologist (OCT) with the task of advancing the state of the art for Mars Entry, Descent, and Landing (EDL) systems. As shown in Fig. 1, the SFDT vehicle will provide the experimental platform necessary for testing three new EDL technologies under simulated Mars-like conditions high in Earth's stratosphere. The enabling technologies under development consist of a new large 33.5 m diameter Supersonic Ringsail (SSRS) parachute and two different types of Supersonic Inflatable Aerodynamic Decelerator (SIAD) devices – a robotic class, SIAD-R, that inflates to a 6 m diameter torus, and an exploration class, SIAD-E, that inflates to an 8 m diameter isotensoid. Stratospheric tests of the SFDT vehicle and their decelerator systems are currently planned for the summers of 2014 and 2015 at the Pacific Missile Range Facility (PMRF) operated by the U.S. Navy on Kauai, Hawaii.

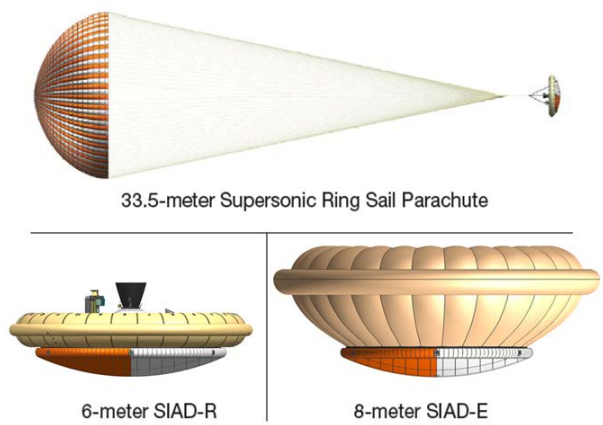

Figure 1. The LDSD project will develop and test two sizes of inflatable aerodynamic drag devices and a large new supersonic ringsail parachute using the SFDT vehicle in a series of high altitude flight tests.[1]

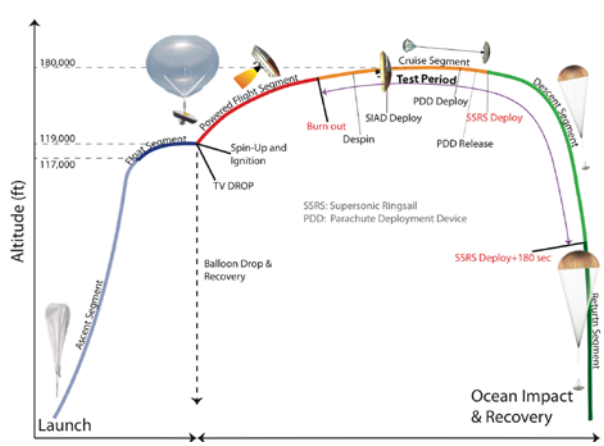

Figure 2. Proposed flight profile for high altitude LDSD test in Earth's stratosphere using the SFDT vehicle.[2]

Figure 2 shows the proposed flight profile for the stratospheric tests which will briefly simulate Mars-like environments while the decelerators are implemented. A large helium carrier balloon provided by NASA Wallops Flight Facility (WFF), and the Columbia Scientific Balloon Facility (CSBF) would lift each SFDT vehicle to a stable float altitude of about 118,000 ft (36 km). Once at altitude, each SFDT vehicle will be released from its carrier balloon and immediately spun up for inertial stability using small solid propellant rocket motors. A separate third stage solid rocket motor will then propel the test vehicle up to an altitude of about 180,000 ft (55 km) and to a speed of approximately Mach 4 in order to achieve the desired scaled test conditions. After main engine burnout, each vehicle will be despun and testing of the deceleration system will begin. First, an inflatable decelerator will be deployed around the aeroshell to dramatically increase the drag surface area and reduce the vehicle speed to approximately Mach 2. A Parachute Deployment Device (PDD) utilizing a mortar in conjunction with a ballute will subsequently pull the 33.5 m SSRS parachute out of the vehicle to complete the vehicle deceleration sequence and ultimately return the vehicle back to the Earth's surface where water recovery operations will begin.

During the early 1970s, NASA performed similar preliminary high altitude testing of the first generation parachute decelerator systems that were eventually used to execute the successful Viking landings on Mars. References 3-6 describe the Balloon Launched Decelerator Test (BLDT) vehicle that was developed for the flight qualification of the Viking parachute system. While the baseline SFDT architecture is very similar to BLDT, the fundamental differences are the additions of a SIAD and a PDD as well as the much faster flight regime, all of which dramatically increase the complexity of the SFDT vehicle design. Previously published papers[2,7,8] have discussed in detail the development of the SIAD-R and SIAD-E concepts as well as the baseline mechanical configuration of the SFDT vehicle. This paper focuses primarily on the thermal design aspects of the SFDT vehicle.

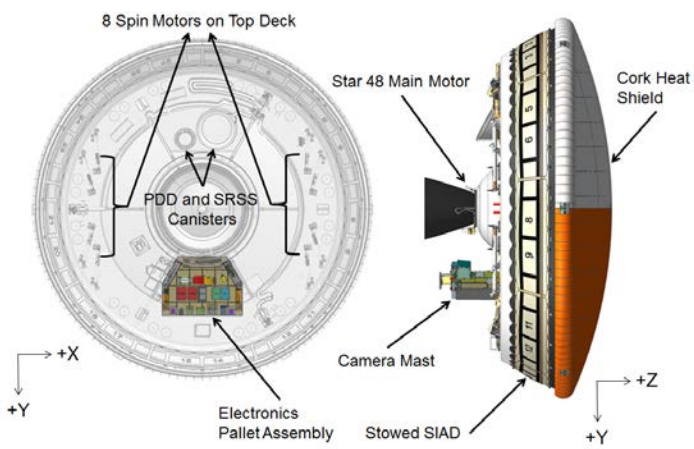

Figure 3. SFDT vehicle, SIAD-R configuration, with electronics pallet assembly location shown.[2]

The SFDT vehicle thermal system must passively protect the vehicle structure and its components from cold temperatures experienced during the ascent phase of the mission as well as from the extreme heat fluxes produced during the supersonic test phase by the main motor plume and aeroheating. Additionally the thermal design must safely reject all of the onboard avionics power dissipation in order to maintain components within their allowable flight temperatures (AFTs). This passive thermal design approach for the SFDT vehicle relies upon careful and complex bounding analysis of all three modes of heat transfer - conduction, convection, and radiation - coupled with a tightly managed transient power dissipation timeline for the onboard electronics throughout all mission phases.

II. SFDT Vehicle Description and Bounding Mission Timelines

Figure 3 shows aft and side views of the SFDT vehicle in the SIAD-R configuration. The vehicle consists of two sets of small spin up and spin down solid rocket motors mounted on the top deck, one 3rd stage Star 48 solid rocket motor used for boosting the vehicle to the desired test altitude and speed, a Camera Mast for collecting visual imagery of the SIAD and SSRS deployments, SRSS and PDD canisters which contain the parachute braking elements, a stowed SIAD flush mounted on the backshell conical surface, a cork heat shield, and an electronics pallet assembly which contains the majority of the onboard avionics necessary to execute the mission. NASA WFF is responsible for providing the electronics pallet assembly. Figure 4 shows an exploded view of the vehicle. Note that the Core Structure Assembly (CSA) is fabricated entirely from composite materials comprised of thin carbon facesheets with a thick Rohacell® foam core. The all composite vehicle structure has made thermal management of the internally dissipating components challenging because the composite material is thermally non-conductive, and acts like an insulating thermos. Additionally the AFT limits for the composites are quite narrow (-43°C to 64°C) as

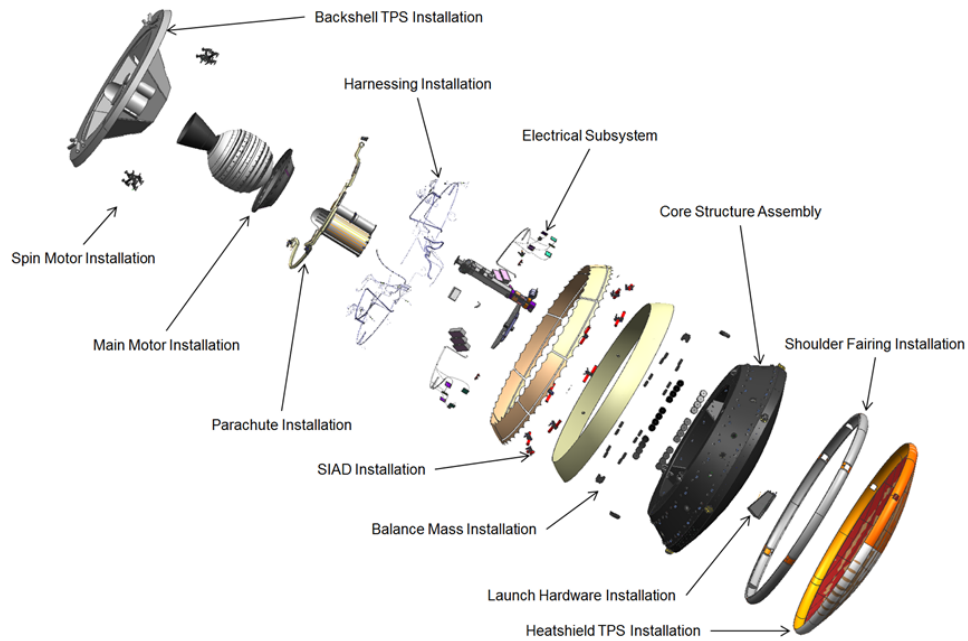

Figure 4. Exploded view of an all composite SFDT vehicle.[2]

compared to what would be acceptable for an all metallic structure (-80°C to 80°C). As a result, a robust Thermal Protection System (TPS) composed of various high temperature insulation blanket arrangements will be installed on the backshell in order to ensure that the CSA is appropriately shielded from the extreme heat produced during the powered flight and LDSD test phases. In addition, the Star 48 main motor will be thermally isolated from the CSA via a stainless steel conical adaptor ring and titanium brackets. Likewise, a cork heat shield will protect the fore body from aeroheating during supersonic flight. There will be several L-band, C-band, S-Band, and UHF antennas underneath the cork covered fiberglass Shoulder Fairing Assembly (SFA) that is attached to the circumference of the vehicle. The antennas will experience cold temperatures during the ascent phase.

The mission timeline as delineated in Table 1 consists of the following phases: Ground Operations (includes two pre-launch avionics functional checkouts and a ready-for-launch power on cycle), Ascent (buoyant helium carrier balloon lifts vehicle to 36 km altitude), Float (stable altitude segment that conservatively allows for up to three power on/off cycles for three balloon release attempts if needed), Powered Flight (balloon release followed by main motor burn to the desired test altitude and Mach number regime), LDSD Test (SIAD and SRSS deploy), followed by Recovery (controlled descent and splashdown of vehicle). The timeline definition is essential to proper thermal management of the SFDT vehicle as it was recognized early on that the avionics will overheat if they are simply left on for longer than is necessary. Table 2 shows the two different sets of assumptions and timelines that bound the thermal analysis. The Worst Case Hot (WCH) analysis timeline assumes an 8:00AM launch where the morning sun is incident on the vehicle while it is staged on the ground prior to launch. The Worst Case Cold (WCC) timeline assumes an earlier launch at 6:30AM, with minimal solar exposure prior to launch, but followed by a longer ascent through the cold troposphere and a shorter float segment. The WCH and WCC analyses assume minimum Current Best Estimate (CBE) mass values for components. The WCH analysis assumes maximum Probable

Table 1. SFDT vehicle WCH mission timeline (8AM Launch).

Mission Phase	Mission Event	Local Time HH:MM:SS	Elapsed Time Sec
Ground Operations	Pre-Lift Checkout, Power ON	4:15:00	0
	Pre-Lift Checkout, Power OFF	5:00:00	2700
	Vehicle Transfer	5:01:00	2760
	Post-Lift Checkout Power ON	6:00:00	6300
	Post-Lift Checkout Power OFF	6:30:00	8100
	Balloon Inflation	6:31:00	8160
	Pre-Launch Power ON	7:30:00	11700
Ascent	Launch	8:00:00	13500
Float	Float Start	10:45:00	23400
	Pre-Release Power ON 1	10:46:00	23460
	Power Down and Hold 1	11:31:00	26160
	Pre-Release Power ON 2	12:01:00	27960
	Power Down and Hold 2	12:46:00	30660
	Pre-Release Power ON 3	13:16:00	32460
	Release	14:01:00	35160
Powered Flight	Spin Up Motor Burn	14:01:00	35160
	Main Motor Burn	14:01:01	35162
	Spin Down Motor Burn	14:02:13	35233
Test	SIAD Deployment	14:02:52	35272
	PDD Deployment	14:04:29	35369
	SSRS Deployment	14:04:43	35383
Recovery	Splashdown	14:51:35	38195

Table 2. Worst case definitions for bounding thermal analysis.

Worst Case Cold (WCC):	Worst Case Hot (WCH):
– longest ascent: 3.75 hr	– shortest ascent: 2.75 hr
– shortest float: 2.25 hr	– longest float: 3.25 hr
– 6:30 AM launch	– 8:00 AM launch
– cold boundary conditions	– hot boundary conditions
– Sky Temperature	– Sky Temperature
– Ground Temperature	– Ground Temperature
– Ambient Air Temperature	– Ambient Air Temperature
– Internal/External Convection	– Internal/External Convection
– Solar/albedo	– Solar/albedo
– CBE power	– PBE power
– CBE mass	– CBE mass

Best Estimate (PBE) dissipations while the WCC analysis assumes minimum CBE power dissipations for the electronics. Additional bounding thermal environments are defined in the next section.

III. SFDT Thermal Environments

Figure 5 depicts the solar, albedo, and infrared (IR) environmental energy exchanges that the SFDT vehicle will experience with its surroundings. Note the SFDT vehicle will be suspended under its carrier balloon at a 24° hang angle and is expected to freely spin ~1 RPM about the gravity vector up until drop. Since the entire mission is within the confines of Earth's atmosphere, an upward and downward IR heat load model is employed to capture the effective sky and ground temperatures. Radiation exchange to altitude dependent sky and ground temperatures as well as convection exchange to the local ambient temperature (T_∞) at altitude are considered. Figure 6 shows additional heat sources during and after powered flight.

Balloon ascent analysis by CSBF provided the enveloping altitude versus time profiles used for the WCC 6:30AM launch and WCH 8:00AM launch as shown in Fig. 7. The direct solar flux considers atmospheric attenuation as dependent upon the local solar elevation angle from the horizon and is also plotted for the two different cases. Figure 8 summarizes all of the WCH and WCC biased thermal boundary conditions that vary as a function of altitude, including the sky IR, ground IR, ambient temperature (T_∞), albedo, and both external and internal convection coefficients. The external convection coefficients are calculated for a sphere with the same surface area as the SFDT vehicle and account for the variations in density with altitude and vehicle velocity. The increase in external convection shown above 36 km is due to the high velocity achieved during powered flight. The internal convection coefficients represent natural convection only within the vehicle interior where the local air flow rates are assumed to be fairly stagnant.

Data from various sources was used to

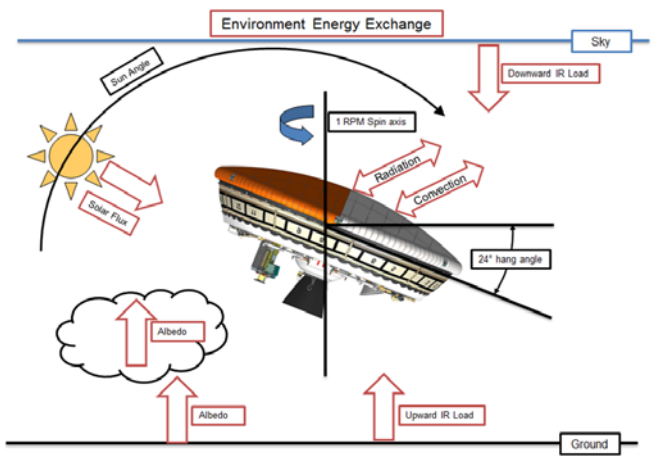

Figure 5. Environmental boundary conditions for the SFDT vehicle as shown in its ascent/float configuration.

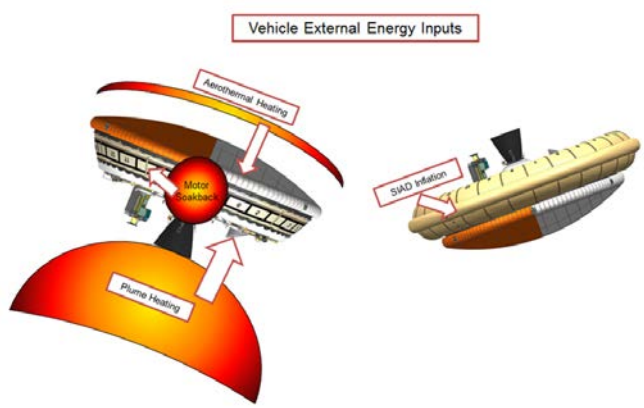

Figure 6. Aerothermal heating, main motor plume heating, main motor soak back heating, and SIAD inflation heating must be carefully considered for the SFDT thermal design.

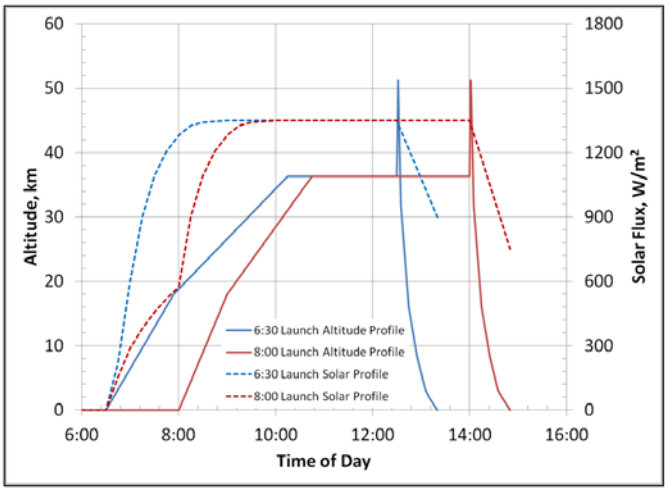

Figure 7. Bounding hot case (8:00AM launch) and cold case (6:30AM launch) altitude and direct solar flux as a function of mission local time.

construct the graph in Fig. 8. Ambient air temperature (T_∞) data was extracted from the Lihue Station Radiosonde data from June through September 2011 since the U. S. standard atmosphere profile does not accurately represent the colder troposphere temperatures typically experienced in the tropics. Sea surface temperature from April through September 2011 is from the Space Science and Engineering Center, University of Wisconsin-Madison. Sky temperature and albedo were extracted from CSBF analysis. The WCC external convection heat transfer coefficients were compared against values that were assumed for the BLDT vehicle thermal design and confirmed to be more conservative.[6] While internal convection was ignored for the BLDT vehicle hot case thermal design, it was more appropriately bounded for the SFDT vehicle in order to realistically assess its relative contribution to a successful passive design.

Figure 9 shows the relative magnitudes and durations of the various heat loads that are imposed on the vehicle post balloon separation due to the mechanisms illustrated in Fig. 6. During the main motor burn which lasts for approximately one minute, a hemispherical shaped plume is expanded out the nozzle with a diameter roughly equivalent to the diameter of the vehicle. The plume imposes severe radiative and convective heat fluxes on the aft end of the vehicle, especially in the vicinity of the top deck where the spin motors are mounted. NASA Marshall Space Flight Center (MSFC) performed a detailed Computational Fluid Dynamics (CFD) analysis to better characterize the interaction between the main motor plume and the SFDT vehicle. While MSFC provided transient convective and radiative heat fluxes for multiple body point locations, Fig. 9 only shows the top deck plume heat flux plotted along with the aerothermal heat flux incident on the cork heat shield as a point of comparison. The plume heating in this location on the aft end of the vehicle is slightly more severe. NASA Ames Research Center (ARC) provided the aeroheating fluxes for the heat shield.

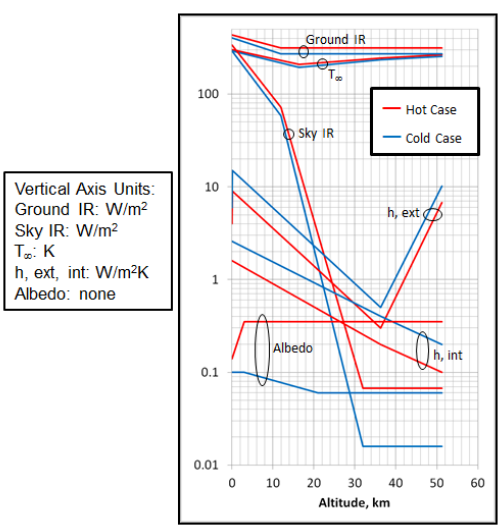

Figure 8. Bounding thermal environments as a function of altitude for the WCH and WCC thermal analyses.

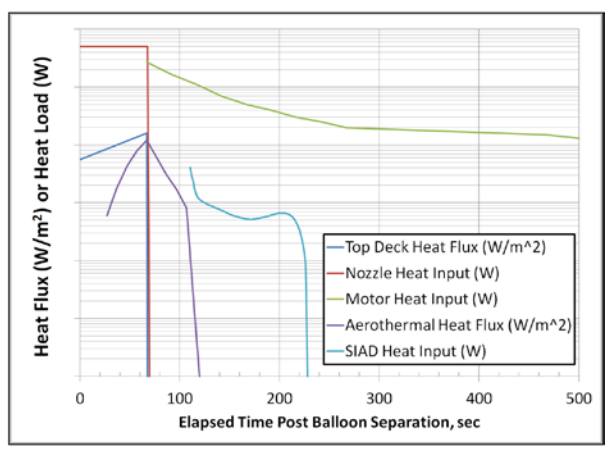

Figure 9. Various heat loads applied to the SFDT vehicle post balloon separation include main motor nozzle and casing heating to simulate engine burn and soak back, plume convective and radiative heating imposed on the backshell, aerothermal heating experienced by the heat shield, and SIAD inflation heating.

The main motor soak back heating starts immediately after the motor burns out and continues all the way until splashdown. This heat load was computed from available ground firing test temperature data furnished by the motor provider, ATK®. The engine casing heats up dramatically and radiates much of the heat toward the vehicle. The backshell TPS must be designed to protect both the CSA and the electronics pallet assembly from this heating.

Figures 6 and 9 also show that SIAD deployment generates significant heating. Onboard gas generators rapidly inflate the SIAD and aerodynamic frictional heating is subsequently conducted, convected, and radiated between outboard and inboard layers of the inflated decelerator where it is ultimately transferred to the composite structure.

IV. SFDT Thermal Analysis

Thermal analysis of the SFDT vehicle was performed using Thermal Desktop®,[9] with the various enveloping boundary conditions described above as inputs to the model. The SFDT Thermal Desktop® model is shown in Fig. 10. Currently, only the electronics pallet assembly and the CSA have been fully analyzed. The camera mast, spin motors, and elements of the parachute system are in the process of being modeled. Thermal Desktop® has a unique tool for analyzing specific trajectories that are a function of longitude, latitude, and altitude and can readily accept inputs for the upward/downward IR atmospheric energy balance model previously described. Also, the fast spin assumption about the gravity vector is easily implemented for averaging the environmental fluxes on the rotating body. Figure 11 shows a picture of the multiple trajectory points that were analyzed for WCH. Thermal Desktop® computes the solar, albedo, ground IR, and sky IR heat loads based upon the calculated view factors between the vehicle, the Earth, and the sky. Internal view factors within the vehicle are computed for all surfaces represented in the model as well. The view from the sun displayed in Fig. 11 reveals that the sun is incident on a large area of the vehicle during the float phase, and warms the vehicle after it ascends through the cold troposphere. There are three main areas discussed in the next section with respect to the thermal design and analysis – the electronics pallet assembly, the CSA, and the main motor mount.

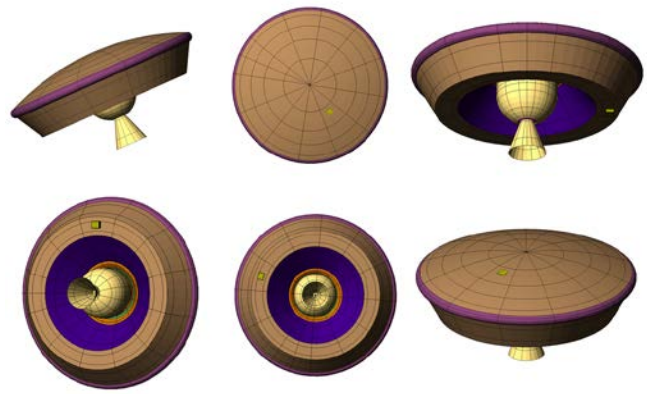

Figure 10. Thermal Desktop® model of the SFDT Vehicle.

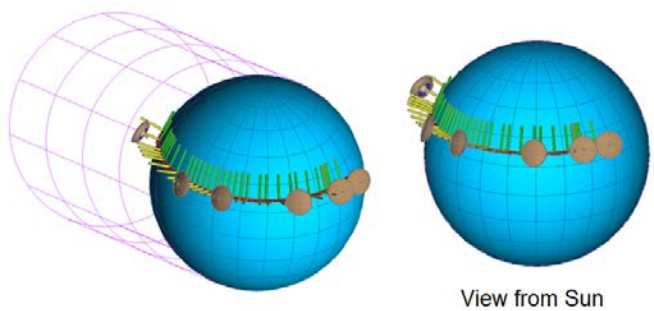

Figure 11. Latitude, longitude, altitude trajectory positions analyzed in Thermal Desktop®.

A. Thermal Analysis of the Electronics Pallet Assembly

Thermal management of the WFF provided electronics pallet assembly is challenging for a number of reasons. Figure 12 shows that there are many components which dissipate a significant amount of heat within small footprints. In particular there are two 20 W transmitters, and one 53 W data encoder. The thermal design approach for the pallet involves passive heat rejection via radiation and natural convection to the surrounding structure. The pallet itself is fabricated from aluminum and is planned to be black anodized. The individual components which are bolted to the pallet will also be covered with black Kapton® tape to increase their emissivity since radiation is the dominant mode of heat transfer at higher altitudes. There are two complicating factors with this passive design

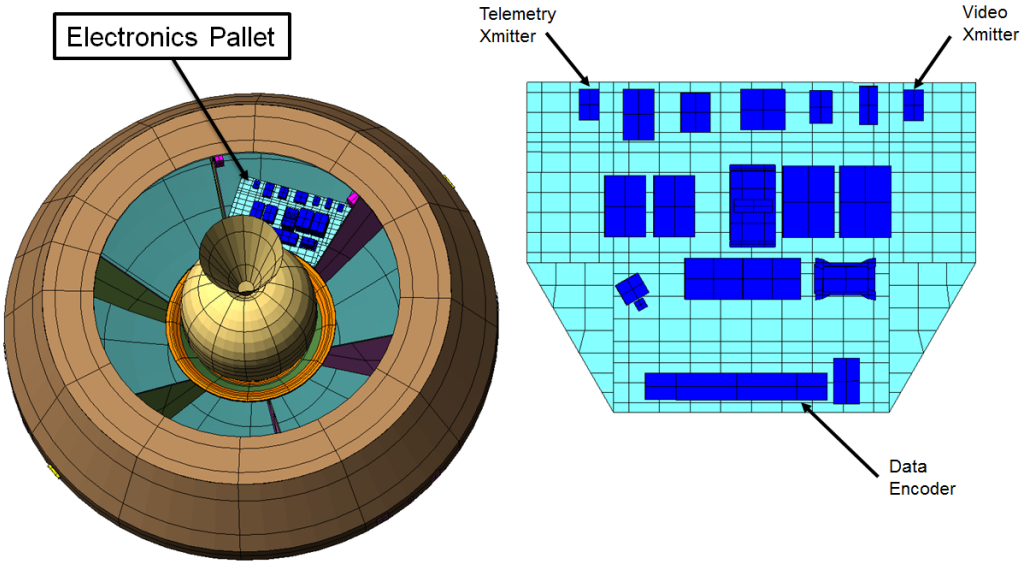

Figure 12. Electronics pallet assembly as modeled in Thermal Desktop®. Note the two transmitters and the data encoder which have significantly high heat fluxes. Cooling fins are provided on the opposite side of the pallet underneath high heat flux components in order to promote passive heat rejection via convection and radiation to the surrounding vehicle structure.

approach: first, due to structural reasons, the pallet must be mounted on top of a composite shelf that has the potential to block half the useful surface area required for effective heat transfer from the pallet, and second, the entire pallet is enclosed within an all composite structure that acts in principle like a thermos.

A number of design features will be employed to extend the operating time of the electrical pallet as much as possible. As shown in Fig. 13, the pallet will overhang the obstructing composite shelf so that components with the highest heat flux have unobstructed views to the surrounding structure. Cooling fins and a thickened pallet underneath the high heat flux components and openings in the composite shelf will be used to maximize heat transfer from the electronics. Furthermore, the CSA bay surrounding the pallet will limit absorbed solar energy by painting the heat shield white in that region. The arrangement of components on the pallet is based upon the dissipative heat flux through their footprint area. High heat flux components are situated next to lower power and more massive components to the extent possible. The transmitters and the encoder are located as far apart from one another as possible and they are located on the overhanging ledges for maximum heat rejection. Additionally, around the perimeter of each component sufficient area was allocated to maximize the radiating footprint. Despite these design features, thermal analysis shows that the electronics cannot be left on indefinitely because they will overheat. To prevent overheating, the electronics equipment will need to be powered on only when needed, and a power conscious timeline must be managed at the system level. The thermal model takes into account the transient dissipation timelines for each of the individual components. Figure 14 shows the total PBE and CBE pallet power profiles assumed for the WCH analysis and WCC analysis, respectively. The CBE values for

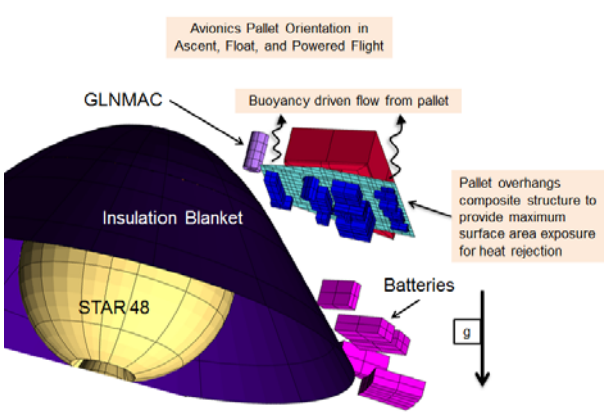

Figure 13. The pallet thermal design passively rejects heat via radiation and natural convection to the nearby surrounding structure.

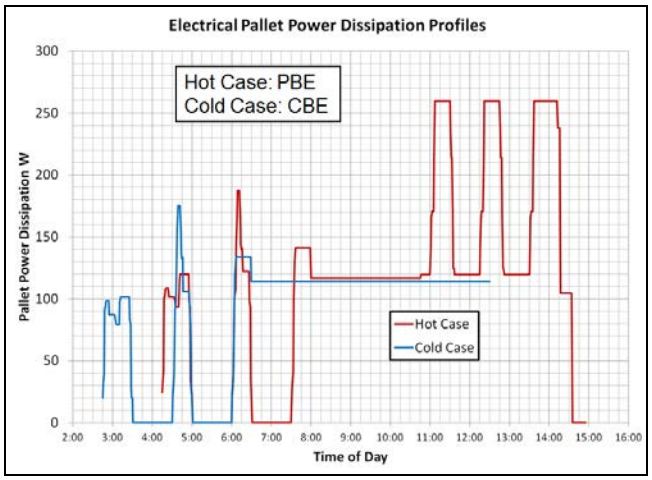

Figure 14. CBE and PBE transient dissipation profiles for the WFF electronics pallet assembly.

Table 3. The temperature requirements for the components on the WFF provided electronics pallet assembly.

SFDT Hardware Thermal Submodel Name	Temperature Requirements, C			
	Allowable Flight			
	Operational		Nonoperational	
	min	max	min	max
Wallops On-Pallet Components				
ATTSW	-39	51	-39	51
CBNDXPNDR	-25	61	-47	75
COLDJNCTN	-40	130	-40	130
CONDCIRC	-25	65	-25	65
CONDCIRC	-14	51	-44	75
CRD1	-39	65	-47	75
CRD2	-39	65	-47	75
EPSU	-25	65	-25	80
FIRINGA	-25	65	-25	65
FIRINGB	-25	65	-25	65
FTSC	-14	51	-24	61
GPSRCVR	-20	55	-25	65
LEDEX	-40	60	-40	60
PWRREG	-20	65	-25	80
RMFT	-14	51	-44	75
SERSRVR1/SERSRVR2	-25	60	-25	65
SERSW	-25	55	-25	65
TRIAX	-40	90	-40	90
TTCENCODR	-40	85	-40	85
TTCRECORD	-20	65	-40	65
VIDCOMBNR	-5	60	-5	60
XMRTVID	-40	85	-40	85
XMTRTM	-40	85	-40	85

mass were modeled for both cases and a conservative value of specific heat was assumed for all of the electronics. Because cable blockage on the top side of the pallet is a serious concern, it was conservatively accounted for in the model by assuming the top side has a low emissivity. Proactive cable management on the top side of the pallet, however, will help to provide additional heat rejection and increase thermal design margin.

Table 3 shows the AFTs for each of the components on the pallet. Some components have narrower AFT limits than others due to the fact that these components are off-the-shelf versus custom components under development.

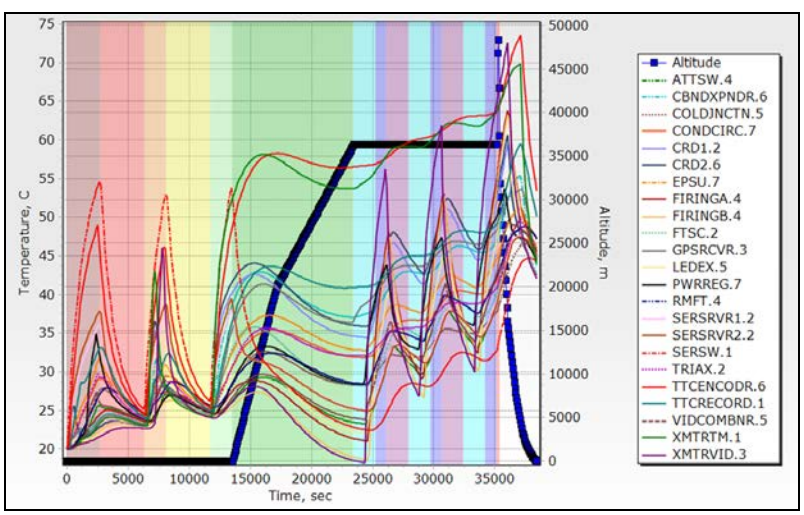

Figure 15. WCH thermal results for the electronics pallet. The various color bands represent the different mission phases – 2 pre-launch tests, ascent, float with 3 drop attempts, LDSD test phase, and descent.

Figures 15 and 16 show the WCH results of all of the components on the pallet. The graphs are color coded by the various mission phases, and an overlay of altitude versus time shows the vehicle position in the mission timeline. Figure 16 essentially shows a zoomed in view of the right hand side of the graph in Fig. 15 to more clearly show the temperature predicts during and after the powered flight and LDSD test phases. The two transmitters (XMTRTM and XMTRVID) and the data encoder (TTCENCODR) are the warmest components. With the current thermal design approach taken, no components exceed their upper AFT limits. After the main motor burn, Fig. 16 shows that the components heat up more rapidly to their peak values due to the motor soak back, until the equipment is eventually powered off. A contour plot in Fig. 17 displays the temperature gradients observed on the pallet around the time when peak temperatures for the data encoder are realized. Figure 18 shows the WCC results for completeness. No minimum AFT limit violations were observed.

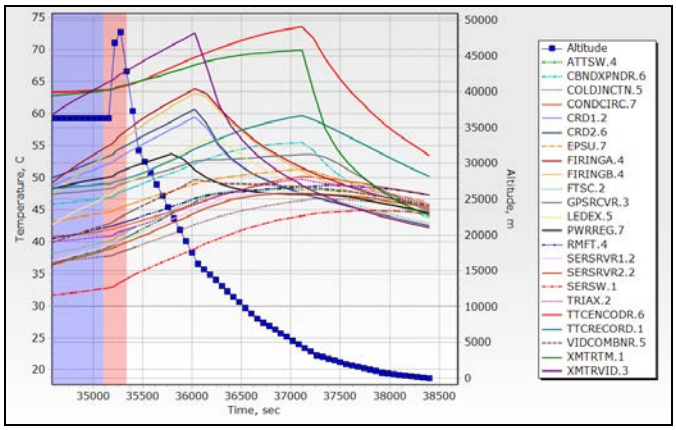

Figure 16. WCH thermal results for the avionics pallet post main motor burn. Red color band signifies powered flight phase until parachute snatch.

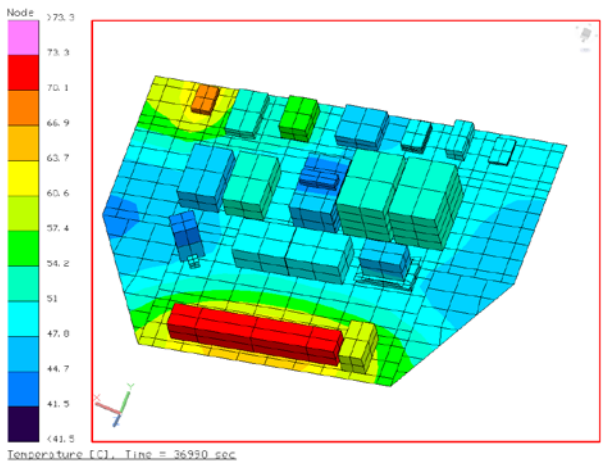

Figure 17. WCH temperature contour plot for the electronics pallet is shown near the time of peak temperature for the data encoder.

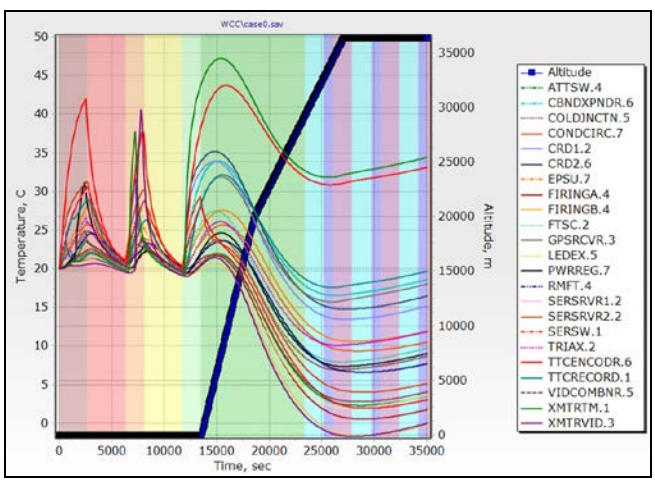

Figure 18. WCC thermal results for the electronics pallet.

B. Thermal Analysis of the CSA

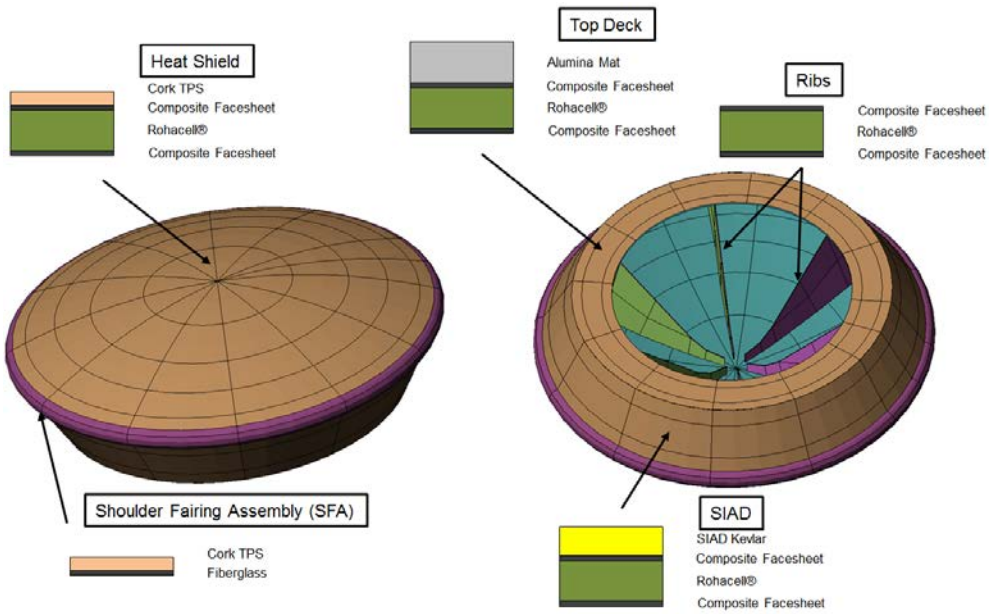

Figure 19. Material layups for the various sections of the CSA.

Figure 19 shows that the CSA consists of five main structural components – the top deck which supports the spin motors, the back shell conic upon which the SIAD is mounted, the heat shield, the SFA, and six interior ribs which segregate the vehicle interior into six equally sized bays and provide the necessary mounting structure for the main motor along the centerline of the vehicle. Schematics of the different material layup configurations are annotated in Fig. 19 for each of the areas above. The thermal analysis of the CSA must carefully assess the through thickness temperature gradients of each of the material stack ups. Conservative thickness estimates of the TPS for the top deck, heat shield, and SFA are paramount to the success of the vehicle surviving the powered flight segment. Also, since there are many internal components on the pallet that must reject heat ultimately through the vehicle structure, heat transfer rates through the composite layers must be analytically determined. Because the top deck, heat shield, SIAD, and SFA all have outer materials with low thermal diffusivity which are subject to short but severe heat fluxes, it is important that an adequate number of nodes be used through the thickness in order to capture peak temperatures on the outer layer. Figure 20 shows that approximately fifty nodes were required through the thickness of the outermost layers in order to assess the maximum material temperatures. Predicts were initially compared to the closed form solution for semi-infinite bodies with a constant heat flux to verify that the model contained appropriate nodal fidelity in these critical regions. The WCH temperature results during and after the powered flight phase are shown for several of the CSA areas on the next page in Figs. 21-26. Each graph displays the maximum AFT as a red horizontal line.

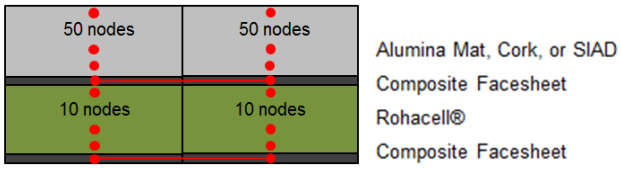

Figure 20. Higher nodal resolution through the thickness is required to capture peak temperatures from aero and plume heating impinging upon low thermal diffusivity material.

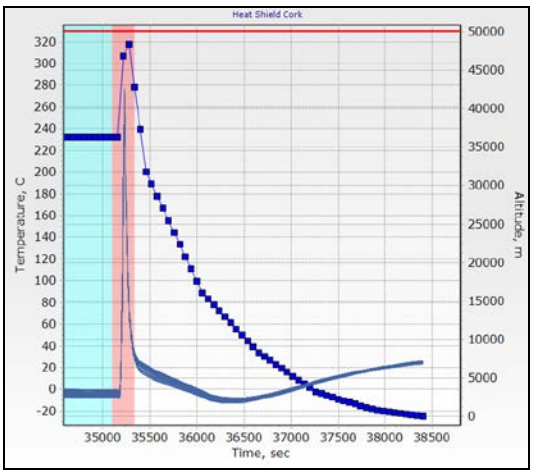

Figure 21. WCH results for the heat shield outer cork layer.

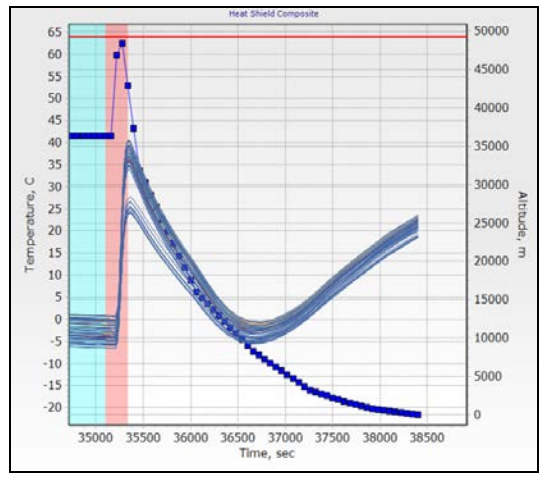

Figure 22. WCH results for the heat shield composite exterior facesheet.

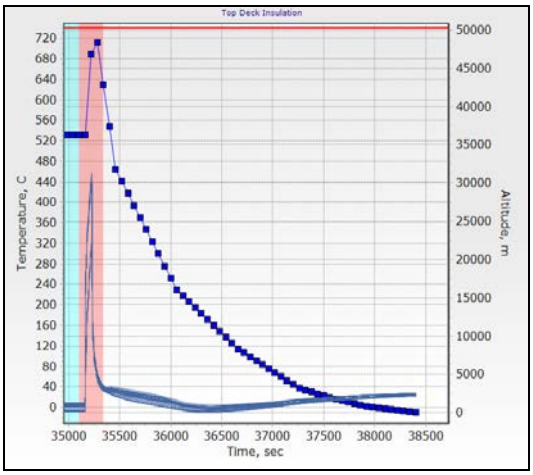

Figure 23. WCH results for the top deck outer insulation layer.

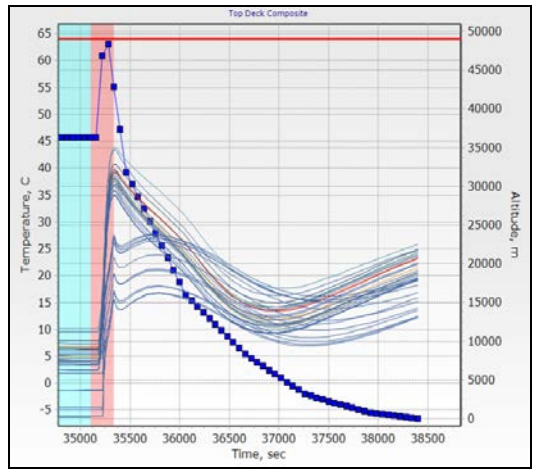

Figure 24. WCH results for the top deck exterior composite facesheet.

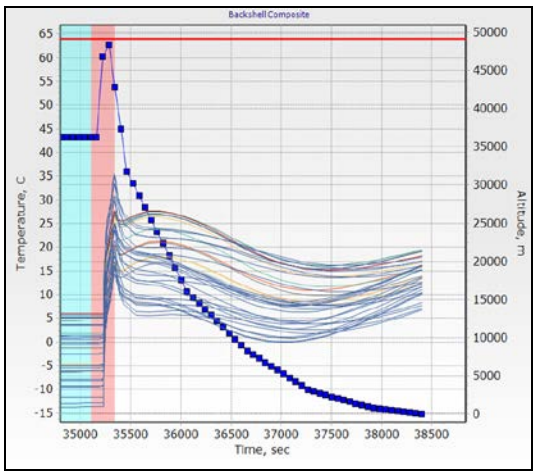

Figure 25. WCH results for back shell exterior composite facesheet underneath the SIAD.

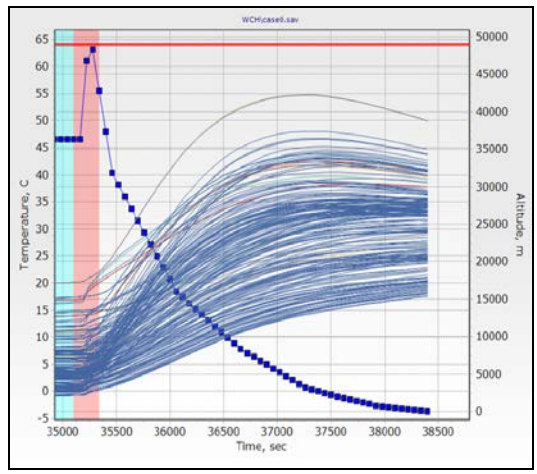

Figure 26. WCH results for the interior ribs.

C. Thermal Analysis of the Main Motor Mount

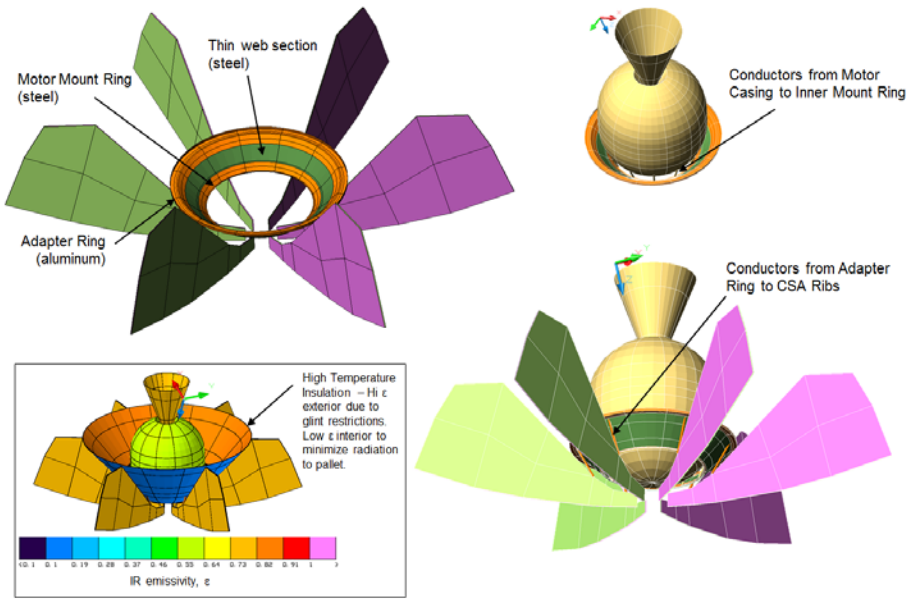

Figure 27. Thermal Desktop® model of main motor mount and insulation shield.

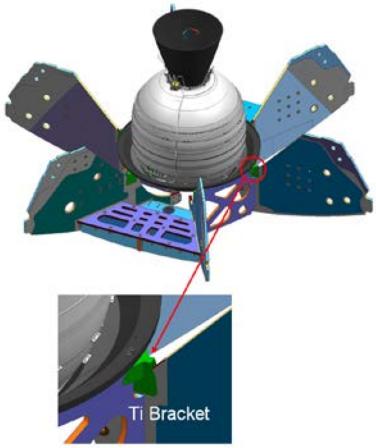

Figure 28. Main motor is thermally isolated from the CSA using a predominantly stainless steel conical mounting ring and titanium brackets.

Figures 27 and 28 show that thermal isolation of the Star 48 main motor from the CSA is achieved using a conical shaped adaptor mount that transitions from a stainless steel inner ring to an aluminum outer ring that is then mated to the CSA via titanium brackets. The motor is radiatively isolated from the rest of the vehicle through the use of a thin high temperature insulation blanket that consists of a low emissivity aluminized layer facing inward and a high emissivity fabric layer facing outward in order to satisfy a low glint requirement that exists within the camera mast fields of view. This insulation blanket effectively shields the structure and the pallet from the high temperatures experienced from plume heating and main motor soak back. WCH results for the motor mount are presented in Figs. 29 and 30. While the inner ring reaches extremely high temperatures, the composite ribs that the motor mount sits on remain well below their maximum AFT limit. Figure 30 shows a temperature contour plot of the main motor mount at parachute snatch which occurs at the right edge of the red color band in Fig. 29.

V. Conclusions

The thermal design of the primarily composite SFDT vehicle has been extremely challenging due to multiple complex and highly transient heat loads that must be passively mitigated. The passive thermal design approach was analytically verified for the pallet assembly, the CSA, and the main motor mount using Thermal Desktop®. All components are currently predicted to meet their allowable flight temperatures.

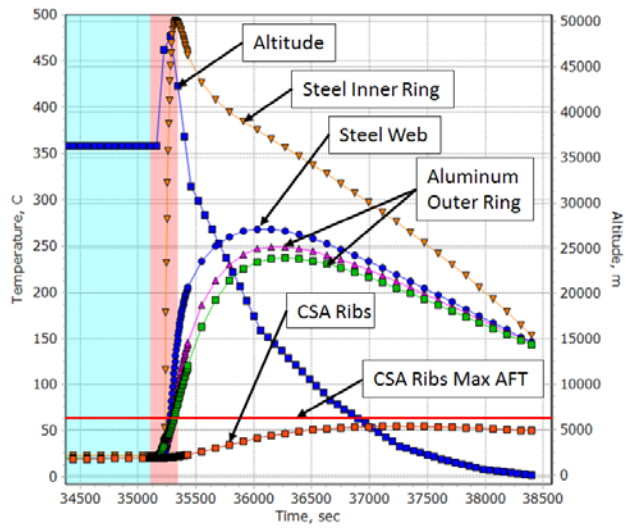

Figure 29. WCH results for main motor mount during and after motor burn. The composite ribs remain below their max AFT limit.

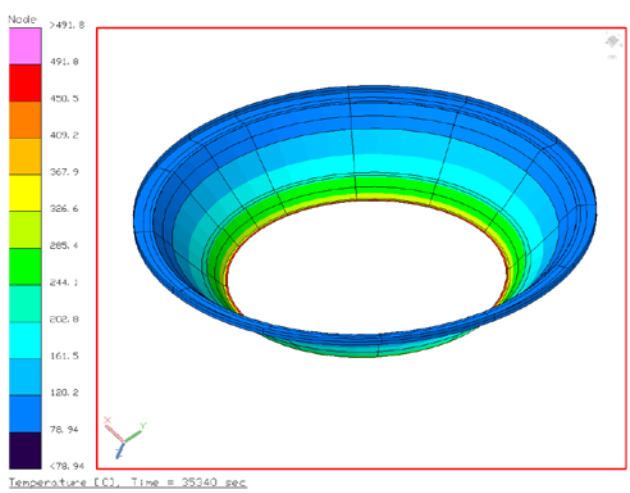

Figure 30. WCH results for motor mount at parachute snatch.

Acknowledgements

The development described in this paper was carried out at the Jet Propulsion Laboratory, California Institute of Technology, under a contract with the National Aeronautics and Space Administration. The authors express their thanks to NASA's Office of the Chief Technologist for supporting this effort and enabling a select few to push the envelope. The authors wish to thank several of their colleagues at JPL who have been instrumental to the thermal design task at hand: Brant Cook, Kevin Burke, John Luke Wolff, Steven Schroeder, George Chen, Jason Gates, Mark Duran, Gabriel Molina, Grace Tan-Wang, Thomas Randolph, Carl Guernsey, Mark Yerdon, Morgan Parker, and Rebekah Tanimoto as well as Virgil Mireles, Tony Paris, Pradeep Bhandari, and Bob Krylo for serving as the thermal review board members. The authors also wish to thank the following individuals from other NASA Centers including Brian Abresch, Joel Simpson, Chris Purdy, Scott Hesh, and Joe O'Brien from WFF and Brandon Mobley (MSFC), Bud Smith (MSFC) and Jay Grinstead (ARC) who provided critical inputs to the SFDT thermal model. Lastly, the authors would like to take this opportunity to acknowledge Mark Welch and Cindy Beer from C&R Technologies® for providing valuable modeling advice.

References

[1]NASA, "Fact Sheet: Low Density Supersonic Decelerators," JPL 400-1530, March 2013, <http://www.nasa.gov/pdf/737628main_Final_LDSD_Fact_Sheet_3-26-13.pdf>.

[2]Cook, B., Blando, G., Kennett, A., Von Der Heydt, M., Wolff, J., and Yerdon, M., "High Altitude Supersonic Decelerator Test Vehicle," 22nd AIAA Aerodynamic Decelerator Systems Conference, Daytona Beach, Florida, March 2013.

[3]Moog, R., Bendura, R., Timmons, J. and Lau, R., "Qualification Flight Tests of the Viking Decelerator System," AIAA-1973-457, AIAA 4th Aerodynamic Deceleration Systems Conference, Palm Springs, California, May 1973.

[4]Raper, J., Lundstrom, R. and Michel, F., "The Viking Parachute Qualification Test Technique," AIAA-1973-456, AIAA 4th Aerodynamic Deceleration Systems Conference, Palm Springs, California, May 1973.

[5]Lundstrom, R., Raper, J., Bendura, R., and Shields, E., "Flight Tests of Viking Parachute System in Three Mach Number Regimes; I: Vehicle Description, Test Operations, and Performance," NASA Technical Note TN D-7692, October 1974.

[6]Buna, T., and Battley, H., "Thermal Design and Performance of the Viking Balloon-Launched Decelerator Test Vehicles," AIAA 1974-760, AIAA/ASME Thermophysics and Heat Transfer Conference, Boston, Massachusetts, July 1974.

[7]Giersch, L., Rivellini, T., Clark, I., Shook, L., Ware, J., and Welch, J., "SIAD-R: A Supersonic Inflatable Aerodynamic Decelerator for Robotic missions to Mars," 22nd AIAA Aerodynamic Decelerator Systems Conference, Daytona Beach, Florida, March 2013.

[8]Coatta, D., Jurewicz, D., Tutt, B., Rivellini, T., and Clark, I., "Development and Testing of an 8 Meter Isotensoid Supersonic Inflatable Aerodynamic Decelerator," 22nd AIAA Aerodynamic Decelerator Systems Conference, Daytona Beach, Florida, March 2013.

[9]Panczak, T., Ring, S., Welch, M., Johnson, D., Cullimore, B., and Bell, D., "C& R Technologies® Thermal Desktop® User's Manual, CAD Based Thermal Analysis and Design, Version 5.5," February 2012.